

# Structural Characterization of the Reaction Pathway in Phosphoserine Phosphatase: Crystallographic “snapshots” of Intermediate States

Weiru Wang<sup>1</sup>, Ho S. Cho<sup>2</sup>, Rosalind Kim<sup>2</sup>, Jaru Jancarik<sup>1</sup>  
Hisao Yokota<sup>2</sup>, Henry H. Nguyen<sup>2</sup>, Igor V. Grigoriev<sup>1</sup>  
David E. Wemmer<sup>1,2\*</sup> and Sung-Hou Kim<sup>1,2\*</sup>

<sup>1</sup>Department of Chemistry  
University of California  
Berkeley, CA 94720-5230, USA

<sup>2</sup>Physical Biosciences Division  
of the Lawrence Berkeley  
National Laboratory, Berkeley  
CA 94720, USA

Phosphoserine phosphatase (PSP) is a member of a large class of enzymes that catalyze phosphoester hydrolysis using a phosphoaspartate–enzyme intermediate. PSP is a likely regulator of the steady-state D-serine level in the brain, which is a critical co-agonist of the *N*-methyl-D-aspartate type of glutamate receptors. Here, we present high-resolution (1.5–1.9 Å) structures of PSP from *Methanococcus jannaschii*, which define the open state prior to substrate binding, the complex with phosphoserine substrate bound (with a D to N mutation in the active site), and the complex with AlF<sub>3</sub>, a transition-state analog for the phospho-transfer steps in the reaction. These structures, together with those described for the BeF<sub>3</sub><sup>−</sup> complex (mimicking the phospho-enzyme) and the enzyme with phosphate product in the active site, provide a detailed structural picture of the full reaction cycle. The structure of the apo state indicates partial unfolding of the enzyme to allow substrate binding, with refolding in the presence of substrate to provide specificity. Interdomain and active-site conformational changes are identified. The structure with the transition state analog bound indicates a “tight” intermediate. A striking structure homology, with significant sequence conservation, among PSP, P-type ATPases and response regulators suggests that the knowledge of the PSP reaction mechanism from the structures determined will provide insights into the reaction mechanisms of the other enzymes in this family.

© 2002 Elsevier Science Ltd. All rights reserved

**Keywords:** phosphotransfer, phospho-monoester hydrolysis; phospho-aspartyl enzyme intermediate; phosphoserine phosphatase; associative mechanism; dissociative mechanism

\*Corresponding authors

## Introduction

Reversible protein phosphorylation plays a central role in regulating basic functions in eukaryotic processes such as DNA replication,<sup>1</sup> cell cycle control,<sup>2,3</sup> gene transcription,<sup>4</sup> protein translation,<sup>5</sup> and energy metabolism. Protein phosphorylation is required also for more complex functions in

higher eukaryotes, such as cell, organ, and limb differentiation,<sup>6</sup> cell survival, synaptic transmission,<sup>7</sup> cell-substratum and cell–cell communication,<sup>8</sup> and to mediate complex interactions with the external environment. Formation and breakage of phosphate monoester bonds are key steps in regulating protein activity.

Over the past four decades, much research effort has been devoted to elucidation of the reaction mechanisms of phosphate monoester hydrolysis, but there has been substantial debate focused on the nature of the transition-state.<sup>9–12</sup> Figure 1 illustrates the two extreme mechanisms proposed; the unimolecular decomposition or dissociative mechanism in which the transition state is thought to be a metaphosphate-like species, and the bimolecular association or associative mechanism

Abbreviations used: PSP, phosphoserine phosphatase; PTP, phosphotyrosine phosphatase; PLS, phospho-L-serine; APUP, aspartyl-phosphate-utilizing phosphohydrolase/phosphotransferase; HAD, haloacid dehalogenase-like hydrolase; NMDA, *N*-methyl-D-aspartate.

E-mail addresses of the corresponding authors: dewemmer@lbl.gov; shkim@cchem.berkeley.edu

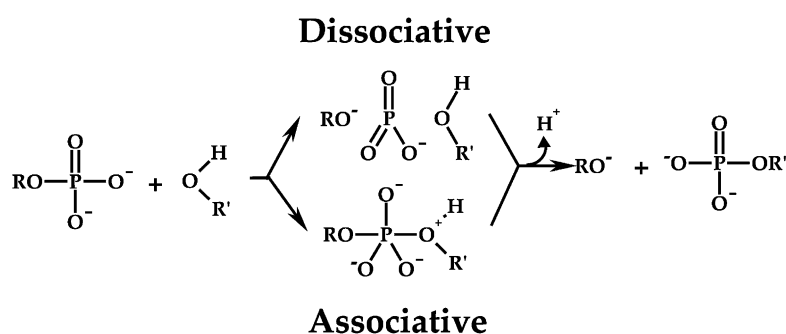


**Figure 1.** The associative and dissociative extremes of phosphomonoester hydrolysis mechanism in PSP.

in which the transition-state is a phosphorane-like pentavalent species. The order and degree of bond breakage/formation determine the nature of the transition-state. Real reactions can range anywhere between the two extremes. The proton can be transferred before or in concert with the nucleophilic attack. Corresponding possible pathways are more complex than shown in this Figure.<sup>13</sup>

Phosphate monoester bonds are usually resistant to hydrolysis under physiological conditions. Hydrolases such as phosphotyrosine phosphatases (PTP)<sup>14</sup> facilitate this reaction by means of nucleophilic catalysis, general acid/base catalysis, and transition state stabilization. Phosphoserine phosphatase (PSP) hydrolyzes phospho-L-serine (PLS) through a stepwise  $Mg^{2+}$ -dependent phosphotransfer mechanism: the phosphoryl group is transferred from PLS to an active-site

aspartate residue of PSP, producing a labile phospho-aspartyl-enzyme intermediate and a serine molecule; the phosphorylated PSP is hydrolyzed subsequently, releasing inorganic phosphate (Pi). Intermediates for such enzymes have been difficult to study experimentally because of the lability of aspartyl-phosphate.

The size of the family of aspartyl-phosphate-utilizing phosphohydrolases/phosphotransferases (APUP) has been increasing. Members of this family possess three consensus sequence motifs. The first motif, DXXX(T/V), in which the first Asp is the site of phosphorylation, is invariant across the family.<sup>15</sup> Two other sequence motifs, motif II, (S/T)XX, and motif III, (G/S)DXX(N/T)D, are highly conserved among most of the family members. The APUP family comprises a subgroup of the haloacid dehalogenase-like hydrolase (HAD) family,<sup>15</sup> which includes phosphatases, phosphomutases, and P-type ATPases. The phosphatases and phosphomutases possess a pattern of DXDX(T/V) in motif I, whereas P-type ATPases are conserved as DKTGT. The receiver domains of two-component signal transduction response regulators have been included into the APUP family on the basis of structural homology.<sup>16</sup>

PSP's product, L-serine, is the precursor of D-serine, the co-agonist of the N-methyl-D-aspartate (NMDA) class of glutamate receptors.<sup>17,18</sup> Mammalian brain development, including the learning process, requires the transmission of electrical signals between neurons *via* the NMDA receptors. NMDA receptor function can regulate neuronal proliferation and migration.<sup>19</sup> PSP is the rate-limiting enzyme in serine biosynthesis, and has been considered a potential regulator of steady-state D-serine level in the brain.

We report here three newly determined, high-resolution structures of PSP as the apoprotein (no  $Mg^{+2}$  or substrate bound), the substrate phosphoserine complex (both with the D11N mutation), and the  $AlF_3$  transition state analog bound. These provide new insights into the mechanism for substrate binding, and for the phosphotransfer reaction mechanism. The new structures complement the previous structures of the  $BeF_3^-$  complex mimicking the phospho-enzyme intermediate,<sup>20</sup> and the phosphate product complex.<sup>21</sup> Together, these let us give a comprehensive structural description of the reaction

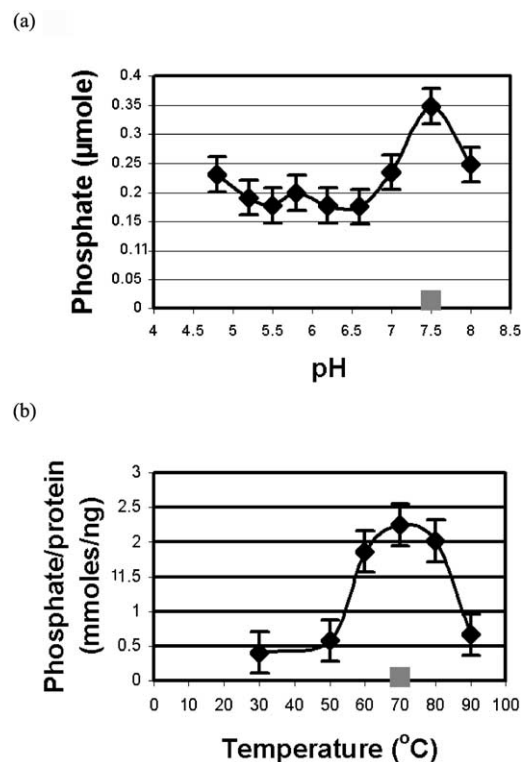


**Figure 2.** Activity assay of wild type PSP and mutant D11N. The D11N activity is denoted as a shaded rectangle.

**Table 1.** X-ray data collection and structure refinement statistics

Parameter	PSP + PLS	PSP + Pi	PSP + AlF <sub>3</sub>	PSP + BeF <sub>3</sub> <sup>-</sup>	Open PSP
<b>A. Data collection</b>					
Space group	P2 <sub>1</sub> 2 <sub>1</sub> 2	P2 <sub>1</sub> 2 <sub>1</sub> 2	P2 <sub>1</sub> 2 <sub>1</sub> 2	P2 <sub>1</sub> 2 <sub>1</sub> 2	P2 <sub>1</sub> 2 <sub>1</sub> 2 <sub>1</sub>
Cell dimensions <i>a/b/c</i> (Å)	70.4/70.8/90.0	69.1/70.3/90.9	69.2/70.6/90.8	68.8/69.8/90.6	36.9/117.4/117.9
Resolution (Å)	20.0–1.9	20.0–1.48	20.0–1.8	20.0–1.5	20.0–2.2
<i>I</i> /σ	15(3.3) <sup>a</sup>	36(3.4)	16(3.3)	16(3.3)	18(5.5)
No. refl.	33257(1679)	72554(3547)	41968(2052)	67186(3066)	25996(1101)
% Complete	94.3(93.3)	98.9(97.4)	99.0(98.7)	93.8(86.5)	98.2(85.3)
<i>R</i> <sub>sym</sub> <sup>b</sup> (%)	4.9(25.1)	3.5(33.5)	6.0(35.8)	6.7(24.8)	7.7(15.8)
<b>B. Structure refinement</b>					
Resolution (Å)	15.0–1.9	15.0–1.48	15.0–1.8	15.0–1.5	15.0–2.2
No. water mol.	193	388	389	402	138
Overall <i>B</i> (Å <sup>2</sup> )	32.40	16.90	18.33	14.77	34.20
<i>R</i> <sub>work</sub> / <i>R</i> <sub>free</sub> (%)	22.9/26.6	20.2/23.2	19.1/22.5	18.9/20.9	22.4/25.4
Bond rmsd (Å)	0.005	0.012	0.013	0.014	0.009
Angle rmsd (deg.)	1.39	1.62	1.67	1.80	1.56

<sup>a</sup> Numbers in parentheses are related to the highest-resolution shell.

<sup>b</sup>  $R_{\text{sym}} = \frac{\sum_{hkl} \sum_i |I_{hkl,i} - \langle I \rangle_{hkl}|}{\sum |I_{hkl}|}$ .

cycle, with five distinct “snapshots” of states during the reaction.

## Results and Discussion

### PSP structures

PSP from *Methanococcus jannaschii* (MJ) and its mutant (D11N) were over-expressed and purified as described.<sup>21</sup> Activity assays indicated that wild-type PSP has a  $V_{\text{max}}$  of 570 min<sup>-1</sup> mg<sup>-1</sup>, a  $K_m$  of 0.62 mM, and a  $k_{\text{cat}}$  of 20 min<sup>-1</sup> at 70 °C and pH 7.5, while the D11N mutant is more than 25-fold less active than the wild-type (Figure 2). The error bar of the data point of the mutant activity runs across the horizontal axis in Figure 2. We have determined the crystal structures of PSP as an apo-enzyme in an open conformation and in complex with PLS (the substrate), AlF<sub>3</sub> (a transition-state analog), BeF<sub>3</sub><sup>-</sup> (a phospho-enzyme intermediate analog), and Pi (the product) (Table 1). D11N allowed us to trap PLS in the active site without hydrolyzing it. The overall PSP structure is composed of two domains; an α/β domain resembling an NAD(P)-binding Rossmann fold and a four-helix-bundle domain. A β-hairpin comprises an extension of the third strand and inserts before the third helix of the α/β domain, and interacts extensively with the helical domain (Figure 3).

PSP active-site residues are at the interface between the two domains. The active site (Figure 4) can be divided into two sub-sites: a phosphate-binding site and a serine-binding site. Lys144, Asn170, Gly100, and a magnesium ion in the phosphate-binding site form a cationic cavity that facilitates the hydrolysis of the phosphate group. All of the phosphate-binding residues are from three conserved sequence motifs. The specificity and orientation of the serine group of PLS are achieved through interactions with residues from the helical domain: Glu20 and Arg56 form H-bonded

salt-bridges with the amino group and the carboxyl group of PLS, respectively, while Met43 and Phe49 form van der Waals contacts with the serine group.

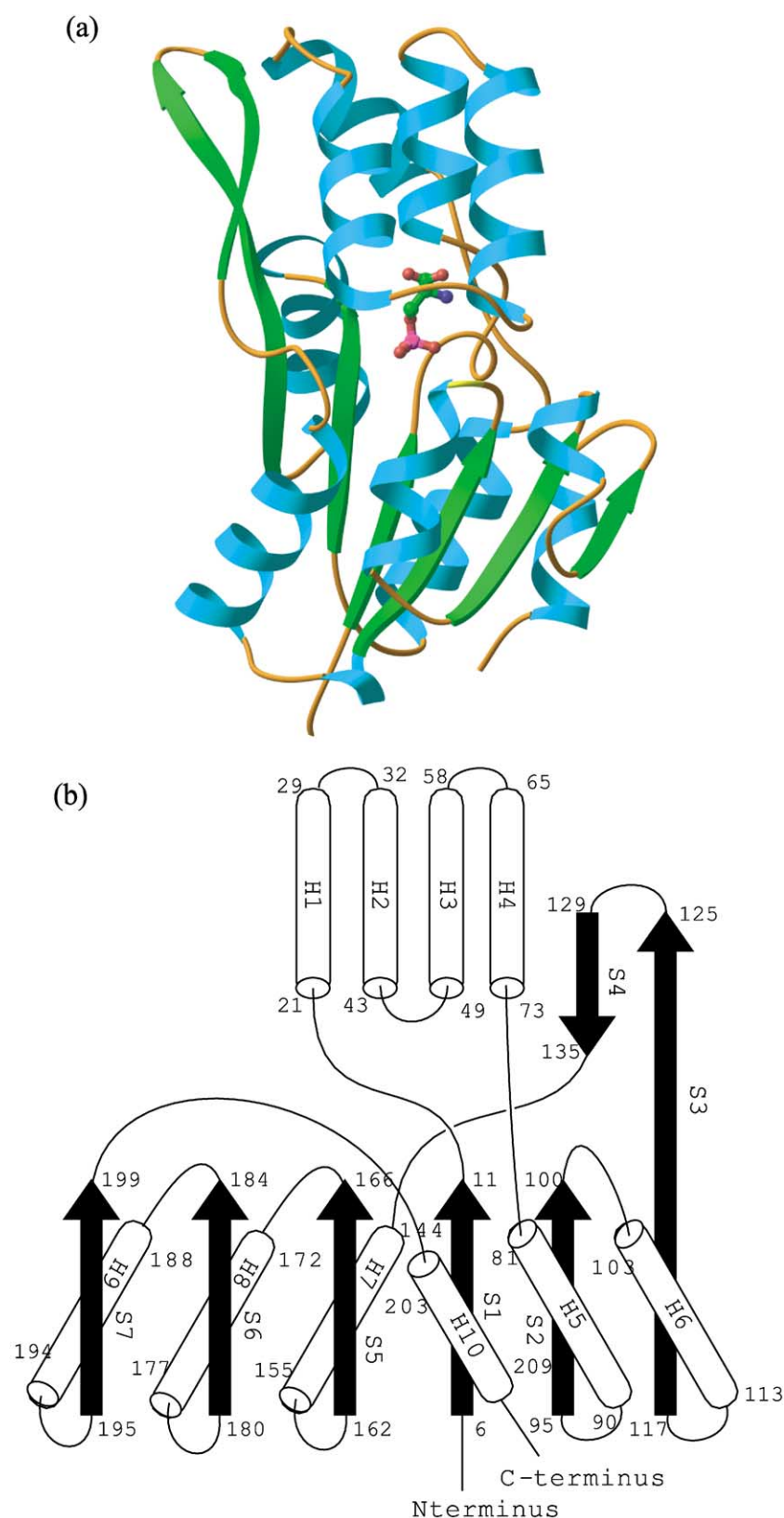
The active site binds one Mg<sup>2+</sup> that is critical for activity and coordinates phosphate directly. The Mg<sup>2+</sup> is hexacoordinated. The other five ligands of the Mg<sup>2+</sup> are the Asp11 side-chain, the Asp13 main-chain carbonyl group, the Asp167 side-chain, and two water molecules. One of the two Mg<sup>2+</sup> ligand water molecules is within H-bond distance of the Glu20 side-chain and Asp13 main-chain carbonyl group, while the other water molecule is within H-bond distance of the Asp11 side-chain, the Asn170 side-chain, the Asp171 side-chain, and the oxygen atom of the Pi that is liganded directly to the Mg<sup>2+</sup>. Motif III residues form a loop structure that chelates Mg<sup>2+</sup> by pointing Asp167 into the Mg<sup>2+</sup>-binding site. Mg<sup>2+</sup> is absent in the D11N mutant active site, probably due to the mutation. Asp171 enhances rigidity of the loop by accepting two H-bonds from NH groups of Gly166 and Asp167. Asp171 communicates with the active site through a salt-bridge from the Lys144 side-chain.

### Structural “snapshots” of the PSP reaction cycle

The PSP reaction proceeds through several intermediate states, as shown in Figure 5(a): the substrate-bound state; a transition state; a phospho-enzyme intermediate state; another transition state; the product-bound state; and finally back to its apo form.

#### Induced fit in the active site when PLS binds to PSP

Structural comparison between the apo-enzyme and PLS–PSP complex reveals an induced fit upon binding of PLS (Figure 4). In both serine and phosphate-binding sites, significant translations



and side-chain rotations occur in the interacting residues, locking the PLS in position. As described below, PSP occludes PLS within the active site at the beginning of the reaction. Asp13 O<sup>δ2</sup> translates by 1.9 Å to form a good H-bond (2.82 Å) with O<sup>γ</sup>

of PLS. Asp13 seems to act as a general acid that donates a proton to stabilize the negative charges developed on the apical oxygen atom upon scissile bond cleavage. As shown in Figure 5(b) II, the amino group of PLS donates an H-bond to the

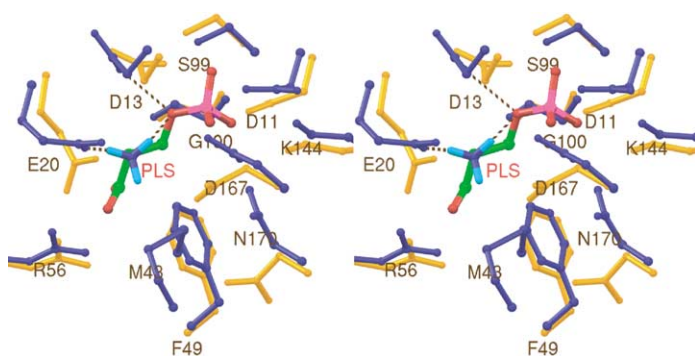


**Figure 4.** Induced fit in the PSP active site upon binding of PLS. Residues of apo-enzyme are colored in gold, residues of PLS bound PSP are colored in dark blue, and PLS is colored by atom type.

apical oxygen atom (2.9 Å) making the serine residue a better leaving group. This H-bond shows a less than ideal geometry with a relatively acute  $N-H \cdots O^\gamma$  angle of  $109^\circ$ . Glu20 also forms a strong H-bond (2.5 Å) with the PLS amino group, which seems to steer the  $NH_3$  group to optimize the H-bond between  $NH_3$  and  $O^\gamma$  of PLS.

#### *The $BeF_3^-$ –PSP-complex as a model for the phospho-enzyme intermediate*

The structure of PSP in complex with beryllium fluoride provides a stable mimic of the phospho-aspartyl-enzyme intermediate.<sup>20</sup> The beryllium atom is bound to  $O^{\delta 1}$  of Asp11 with a bond length of 1.55 Å.  $O^{\delta 1}$  and three fluorine atoms display a nearly ideal tetrahedral geometry that is inverted from that of the phosphate group of PLS, its substrate. The three fluorine ions essentially superimpose the three equatorial oxygen atoms of the phosphate group. They also form the same set of H-bonds with active-site residues. Three water molecules WatB1, WatB2 and WatB, replace the amino group, carboxyl group, and  $O^\gamma$  of PLS, respectively, in the serine-binding pocket (Figure 5(b) IV). WatB is co-linear with the  $Be-O^{\delta 1}$  bond. It is positioned to be the attacking nucleophilic water molecule that should perform an in-line attack on the aspartyl-phosphate group. It may occupy the same position as the serine  $O^\gamma$  after the phosphotransfer reaction. Asp13 is well positioned to act as a general base activating the nucleophilic water molecule. Activation of the attacking water molecule is crucial to the overall reaction, to ensure that the phosphate displacement step is not rate-limiting. In PTP1B, positioning of the nucleophilic water molecule is done by Gln262 and the general base Asp181.<sup>22</sup> A similar scenario is seen in the Ras complex.<sup>23</sup> No residue comparable to Gln262 of PTP1B is found in PSP. Instead, WatB forms H-bonds to Asp13, WatB1, and WatB3, another water molecule in the catalytic site. The  $C^\alpha$  atom of Gly100 contributes van der Waals contacts to WatB. These interactions seem to facilitate positioning of the nucleophilic water molecule. Glu20, a highly conserved residue among PSPs, interacts with WatB through WatB1, suggesting that Glu20 may assist the attacking water molecule indirectly.

#### *Pi complex structure, product-bound PSP*

In the Pi complex (Figure 5(b) VI), the main-chain and the side-chain conformations of the active site are very similar to those in the  $BeF_3^-$  bound PSP (Figure 5(b) IV) except for two residues. The  $Mg^{2+}$  ligand Asp167 shows a different  $\chi_2$  torsion angle, which is  $90^\circ$  away from that found in  $BeF_3^-$ –PSP complex. Asp11, the site of phosphorylation, adopts two conformations; conformer I and conformer II, with  $O^{\delta 1}$  to phosphorus atom distances of 2.75 Å and 4.43 Å, respectively.

A comparison between the Pi complex and the PLS complex reveals interesting similarities. In spite of the fact that the PLS complex used the D11N mutant, the Pi essentially superimposes the phosphate group of PLS. In addition, the structure alignment based on a difference distance matrix plot (DDMP)<sup>24</sup> indicates that the main-chain conformation of the Pi complex is more similar to that of the PLS complex than the other complex structures. The Pi complex structure, therefore, highly resembles the phosphoserine-bound state, which is consistent with the previous postulation.<sup>21</sup>

#### *The $AlF_3$ –PSP complex structure as a transition state structure model*

Aluminum fluoride binds to the PSP active site as a mixture of  $AlF_3$  and  $AlF_4^-$  in the co-crystals. However, there is no detectable conformational heterogeneity in any of the active-site residues at 1.8 Å resolution. The trigonal plane of  $AlF_3$  sits in a position between Pi and  $BeF_3^-$ , with the three fluorine ions closely superimposing the three equatorial oxygen atom positions. The Al atom is exactly co-linear with the coordination water molecule (WatA) and Asp11  $O^{\delta 1}$  (Figure 5(b) V). The side-chain of Asp11 adopts a single conformation, which overlaps one of the two conformers in the Pi complex. The position of WatA, equivalent to WatB in the  $BeF_3^-$ –PSP complex, is positioned to be the attacking water molecule during the dephosphorylation reaction and may also resemble the position of the transition state serine  $O^\gamma$  during the phosphotransfer reaction. WatA forms H-bonds with Asp13  $O^{\delta 1}$  (2.55 Å) and WatA1 (2.82 Å), equivalent to WatB1. WatA1, in turn, H-bonds with Glu20  $O^{\delta 1}$  (2.63 Å), providing

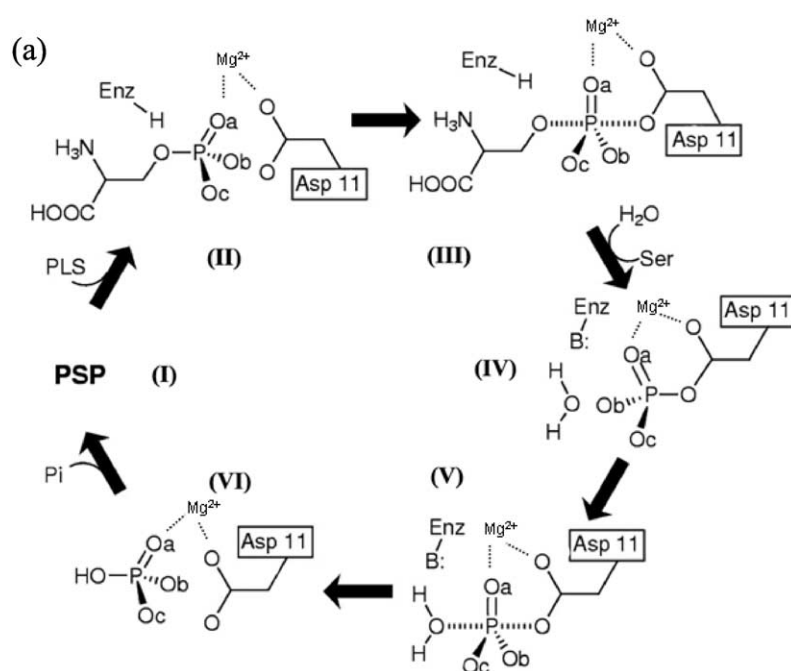


Figure 5 (legend opposite)

additional evidence that Glu20 assists in the nucleophilic attack and stabilization of the transition state. The short H-bond between WatA and Asp13 (2.55 Å) was also short in PO4 complex, O4 to Asp13 (2.57 Å), but not so short in BeF complex, WatB to Asp13 (2.81 Å). The H-bond WatA1 to Glu20 (2.63 Å) was relatively short in BeF complex (2.67 Å), but not short in the PO4 complex WatP1 to Glu20 (2.80 Å). The pattern of changes in H-bond lengths of the water molecules may or may not be important mechanistically.

#### Open and closed forms of PSP

Significant conformational differences are observed when comparing the open form of PSP to the closed form (Figure 6(a)). In the open form, the last two turns of helix H2 and the following loop (Lys40 to Leu47) were not visible in the electron density map, indicating that the structure was destabilized in this region. The inter-domain H-bond between Ala196 CO and Met43 NH (2.93 Å) no longer exists. As shown in Figure 6(b) and (c), destabilization of the H2-loop region effectively opens the active site. The B-factor profile (Figure 6(d)) indicates that the four-helix domain and the  $\beta$ -hairpin are much more mobile in the open form than in the closed forms. A structural alignment of the open form relative to the closed form reveals that the four-helix-bundle domain can alter its position *via* a hinge motion. Two hinge points, as shown in Figure 6(a), are located around Asn18 and Pro77. The  $\beta$ -hairpin seems to move in concert with the helical domain. Relatively minor loop motions are observed in the  $\alpha/\beta$

domain as well, which are generally consistent with the induced fit in the active site as described above.

#### PSP reaction mechanism

The high resolution structural "snapshots" (Figure 5(b)) provide a detailed understanding of the PSP reaction pathway. Most of the previously reported kinetic results<sup>25</sup> can be explained on the basis of the structural data.

The overall PSP reaction requires a dynamic structure. In the absence of substrate or product, the PSP structure is open. Opening occurs through flexibility in the helix H2 and the following loop, which cover the active site. Binding of PLS stabilizes the overall structure in a closed state through contacts of residues in the helix to the serine residue, which facilitates the phosphotransfer reaction. After the phosphotransfer occurs, the active site must open to release serine and let three water molecules enter. Glu20 is important to both steps of the reaction. It arises from the four-helix-bundle domain, suggesting that this domain must be positioned correctly in the closed states to ensure the function of Glu20. After hydrolysis of the phospho-aspartate, the structure must again open to release phosphate and allow a new substrate to enter.

In light of the structural results, it becomes clear that the PSP reaction involves nucleophilic attacks with acid/base catalysis. Two highly conserved residues, Asp13 and Glu20, are critical to the acid/base catalysis. In the phosphotransfer reaction, Asp13 serves as the general acid donating a

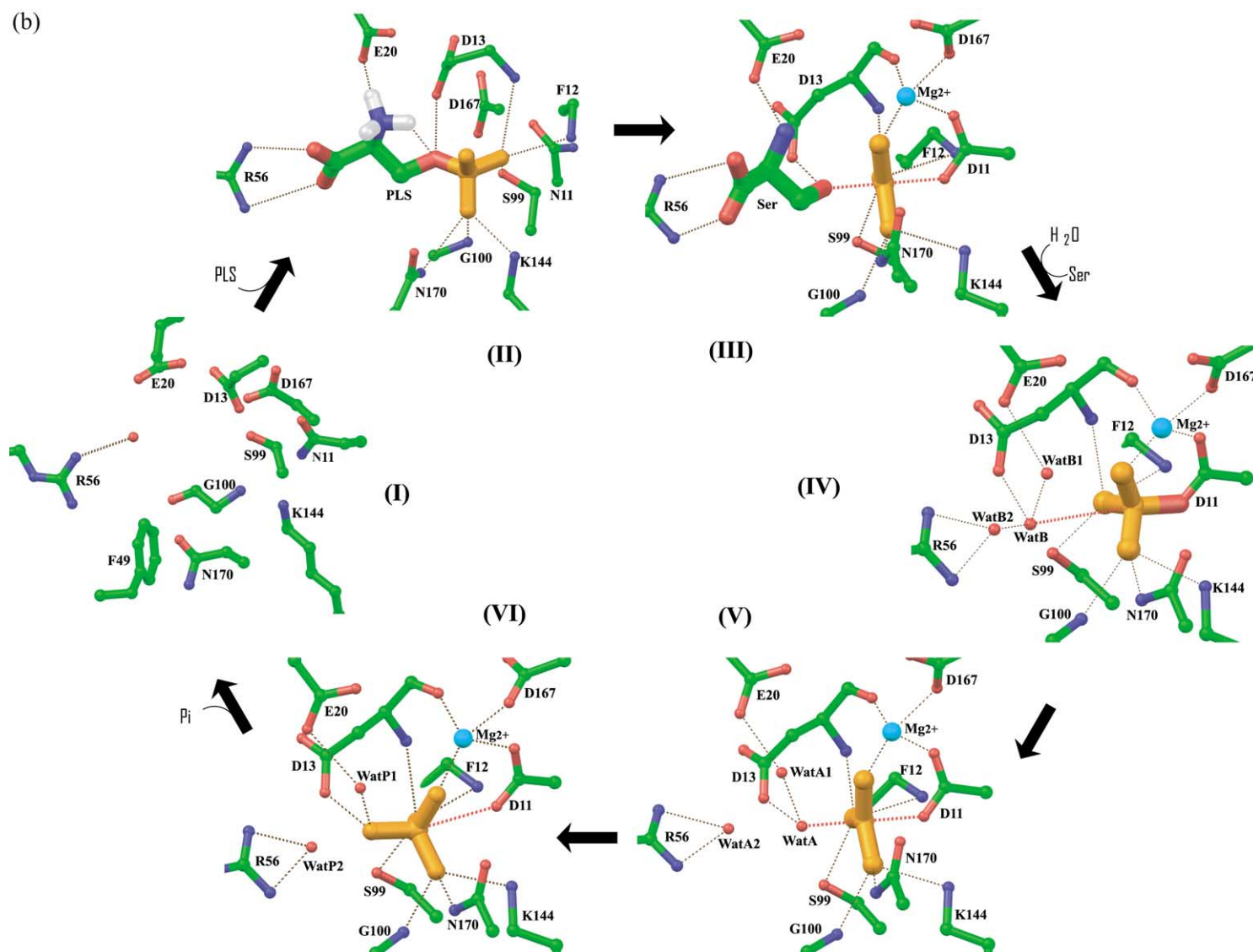


**Figure 5.** Structural “snapshots” of the PSP reaction cycle in the active site. (a) The PSP reaction cycle. (b) Structure and models in the active site. (I) The apo-enzyme structure. (II) The substrate, PLS, bound structure, using mutant D11N. (III) The model of Ser bound transition state structural analogue. A Ser molecule was modeled in the  $AlF_3$ -PSP active site. (IV) Phospho-aspartyl enzyme intermediate structural analogue. The PSP +  $BeF_3^-$  complex. (V) The transition state structural analogue.  $AlF_3$ -PSP complex. (VI) The product,  $P_i$ , bound structure.

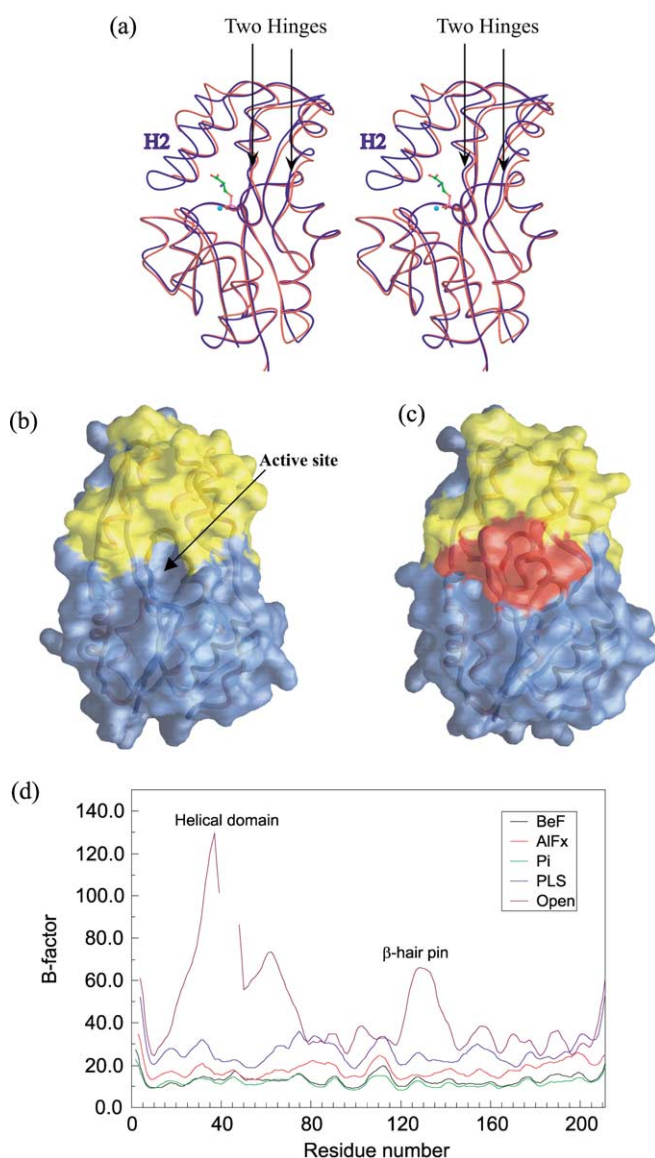


**Figure 6.** Comparison of open and closed forms of PSP. (a) A Ribbon diagram superposition of PSP open (red) and closed (blue) forms. (b) A surface representation of PSP in the open form. The  $\alpha/\beta$  domain is colored in blue, the four-helix-bundle domain is colored in yellow. (c) The surface representation of PSP in closed form. The  $\alpha/\beta$  domain is colored in blue, the four-helix-bundle domain is colored in yellow, and the stabilized loop is colored in red. (d) The *B*-factor profiles of the PSP structures. The values reflect averaged main-chain *B*-factors.

proton to the leaving group. Glu20 seems to enhance the leaving group by orienting the amino group of PLS for substrate assistance. During the dephosphorylation reaction, Asp13 acts as the general base, extracting a proton from the attacking water molecule. Glu20 assists indirectly by positioning this nucleophilic water molecule.

The transition state analogue complex is much tightened compared to the starting point of the reaction. In the phosphotransfer step, PLS binds, presenting the phosphate group in close proximity to Asp11 O<sup>61</sup>, the nucleophile. The Asp11 side-chain seems to adopt two conformations with O<sup>61</sup> to phosphorus atom distances of 4.28 Å and 2.90 Å, respectively, and an average distance of 3.59 Å. This distance shortens to 2.09 Å in the transition state, mimicking the AlF<sub>3</sub>-PSP structure. During this step, the distance between the attacking water molecule and the aluminum (phosphorus) center shortens from 3.56 Å to 2.16 Å.

The transition state seems to be stabilized by an interaction with a positively charged cavity comprised of Lys144, the magnesium ion, and other groups (Asp170 side-chain, Phe12 main-chain NH, Asp13 main-chain NH, and Gly100 main-chain NH) around the phosphate-binding site. Mutagenesis studies on human PSP<sup>25</sup> showed that the positive charges at the catalytic site are essential for activity. Although such charge stabilization has been invoked to indicate a more associative reaction mechanism (which develops more charge on the intermediate), this has not been borne out in isotope effect and linear free energy relationship studies.<sup>26–28</sup> In the present case, the reaction coordinate distances of 3.59 Å and 3.56 Å are less than the 4.9 Å estimated for the fully dissociative mechanism,<sup>12</sup> suggesting that the mechanism could be associative. Since distances and specific charge distribution could be different in the real transition state, this view will have to await

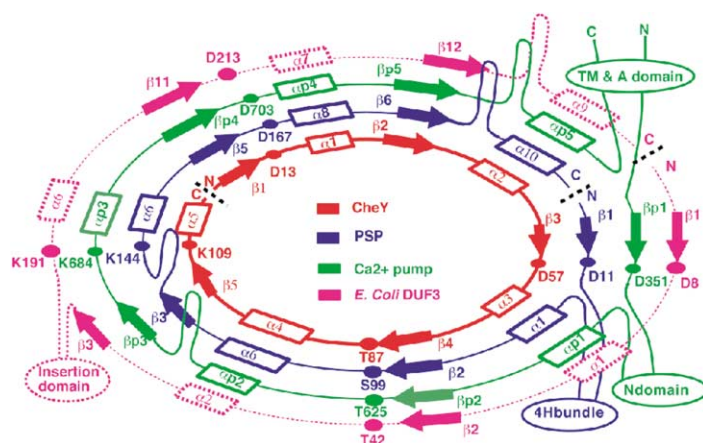


**Figure 7.** A circular presentation of secondary structure alignment among PSP (blue), CheY (red),  $\text{Ca}^{2+}$ -ATPase (green), and *E. coli* DUF3 (gi1724027) (magenta).

verification through isotope effect studies on the real reaction.

In summary, the PSP structures with the transition state and reaction intermediate analogues bound suggest tightening of the transition state analogue complex compared to the starting state. However, the structure and charge distribution of the  $\text{BeF}_3^-$  and  $\text{AlF}_3$  complexes is not identical with that of the actual transition state, further studies that investigate the transition state directly are necessary to elucidate the reaction mechanism.

### Structural similarity allows one to suggest a PSP reaction mechanism to APUP family members

The  $\text{Ca}^{2+}$ -ATPase P-domain<sup>29</sup> and the receiver domain of response regulators<sup>30–37</sup> have a fold similar to that of the  $\alpha/\beta$  domain of PSP (Figure 7) with their catalytic residues extensively superimposable. The phosphate monoester hydrolysis reaction utilizes a stepwise  $\text{Mg}^{2+}$ -dependent mechanism with reversible phosphorylation at an Asp in the active site<sup>38,39</sup> similar to that of PSP. Structural homology suggests a similar mechanism is utilized for catalysis.

Recently, the C-terminal domain phosphatase (Fcp1p), a regulator of RNA polymerase II activity,<sup>40</sup> and Psr1p/Psr2p gene products, novel regulators of salt stress response in yeast<sup>41</sup> were identified to have strong DXDX(T/V) sequence-dependent phosphatase activity, hence they are likely to be APUP members. Another example, the product of the *cicA* gene from *Caulobacter crescentus*, which is essential for cell growth and normal morphology, possesses significant sequence homology in the three conserved motifs. Mutation studies indicated that several key residues in the sequence motifs are catalytically important, providing strong indication that *cicA* also belongs to the APUP family.<sup>42</sup>

A database search revealed that sequences of domains of unknown function (DUF3) from prokaryotic cells possess all three consensus motifs as well as similar regions of secondary structural arrangement (Figure 7), strongly suggesting a

phosphotransfer-related activity as the DUF3 function.

## Materials and Methods

### Enzyme activity assay

MJ PSP was expressed, purified and crystallized as described.<sup>21</sup> To determine the optimum pH for the wild-type PSP, the following buffers were used at a final concentration of 50 mM: sodium acetate, pH 4.8; sodium acetate, pH 5.2; sodium acetate, pH 5.5; imidazole, pH 6.2; imidazole, pH 6.6; imidazole, pH 7.0; Hepes, pH 7.5; Tris, pH 8.0 (Figure 2(a)). The optimum temperature for wild-type PSP was determined by the above assay in 50 mM Hepes (pH 7.5) at different temperatures: 30 °C, 50 °C and 90 °C using 400 ng of PSP, and at 60 °C, 70 °C and 80 °C using 30 ng of PSP: PSP activity was assayed essentially as described by Fallon<sup>43</sup> but with modifications (Figure 2(b)). The assay was performed in a final volume of 0.25 ml consisting of each of the above buffers, 5 mM  $\text{MgCl}_2$ , 3 mM EDTA, 1 mM DTT, 1 mM O-phospho-L-serine and 200 ng of wild-type PSP. The reaction was terminated after 20 minutes of incubation at 70 °C by addition of 0.1 volume of ice-cold 40% (w/v) trichloroacetic acid followed by incubation on ice for 30 minutes before centrifugation at 3000g. Inorganic phosphate present in the supernatant was assayed using the method developed by Chen.<sup>44</sup> D11N assay was done at pH 7.5, 70 °C, using 200 ng of D11N. The enzyme was saturated with substrate during the measurement.

### Crystallization and structure determination

The PSP complex crystals were obtained by co-crystallization using previously described conditions<sup>21</sup> with modifications.  $\text{Mg}^{2+}$  was present at 5 mM. Phospho-L-serine was co-crystallized with mutant D11N to ensure a stable Michaelis complex.  $(\text{NH}_4)_2\text{SO}_4$  was used instead of  $\text{Na}_3\text{PO}_4$  for the PLS complex crystals. Optimal ratios of  $\text{BeCl}_2\text{:NaF:PSP}$ ,  $\text{AlCl}_3\text{:NaF:PSP}$ , and  $\text{PLS:PSP(D11N)}$  were obtained by NMR experiments.<sup>20</sup> The open form crystals were grown with the D11N mutant in 0.1 M cacodylate buffer (pH 7.4), 20 mM zinc acetate, 10% (w/v) PEG 3350. The X-ray diffraction data were collected under cryogenic conditions at the Advanced Light Source beamline 5.0.2 using a Quantum-4 CCD detector. The data were reduced using program DENZO/SCALEPACK.<sup>45</sup> The open form PSP structure

was determined by molecular replacement methods using the program AMoRe.<sup>46</sup> The  $\alpha/\beta$  domain and four-helix-bundle domain of the closed form structure 1F5S,<sup>21</sup> were used as two separate search models. Structure refinement was performed using program CNS.<sup>47</sup> The protein portion of 1F5S was taken as a starting model for refinement of PSP complexes. Rigid body refinement was first applied at 3.5 Å resolution followed by torsion angle dynamics and simulated annealing procedures at maximum resolution. Subsequent positional refinement, individual *B*-factor refinement, and manual fitting using the program O<sup>48</sup> were performed iteratively. Ligands and water molecules were gradually built into the structures through the refinement process. In the structure of PSP +  $\text{AlF}_x$  complex, electron density indicated that aluminum fluoride bound to the PSP active site in both  $\text{AlF}_3$  and  $\text{AlF}_4^-$  forms with a respective occupancy of 0.4 and 0.6, and comparable *B* factors. The X-ray data collection and structure refinement statistics are shown in Table 1.

### Protein Data Bank accession codes

Coordinates and structure factors have been deposited in the Protein Data Bank (PDB). The PDB codes for PSP +  $\text{BeF}_3^-$  complex, PSP + Pi complex, PSP +  $\text{AlF}_x$  complex, apo-enzyme, and PSP + PLS complex, are 1J97, 1L7M, 1L7N, 1L7O, and 1L7P, respectively.

### Acknowledgments

We thank Dr Dalai Yan and Dr Sydney Kustu for help in the beryllium fluoride and aluminum fluoride methods, Dr David King for performing mass spectrometry on the PSP samples, Dr Thomas N. Earnest and Dr Gerry McDermott for assistance during data collection at the Advanced Light Source, Lawrence Berkeley National Laboratory, Berkeley CA, and Dr Ashley Deacon for advice on data reduction. This work was supported by the Director, Office of Science, Office of Biological and Environmental Research under US Department of Energy Contract no. DE-AC03-76SF00098 (to S.-H.K. and R.K.), and by National Institutes of Health (P50 GM62412 to S.-H.K. and R.K., and GM62163 to D.E.W.).

### References

- Muzi-Falconi, M., Brown, G. W. & Kelly, T. J. (1996). Controlling initiation during the cell cycle. DNA replication. *Curr. Biol.* **6**, 229–233.
- Parsons, G. G. & Spencer, C. A. (1997). Mitotic repression of RNA polymerase II transcription is accompanied by release of transcription elongation complexes. *Mol. Cell Biol.* **17**, 5791–5802.
- Wilkinson, M. G. & Millar, J. B. (2000). Control of the eukaryotic cell cycle by MAP kinase signaling pathways. *FASEB J.* **14**, 2147–2157.
- Dahmus, M. E. (1994). The role of multisite phosphorylation in the regulation of RNA polymerase II activity. *Prog. Nucl. Acid Res. Mol. Biol.* **48**, 143–179.
- Sarre, T. F. (1989). The phosphorylation of eukaryotic initiation factor 2: a principle of translational control in mammalian cells. *Biosystems*, **22**, 311–325.
- Schlessinger, J. & Ullrich, A. (1992). Growth factor signaling by receptor tyrosine kinases. *Neuron*, **9**, 383–391.
- Greengard, P. (2001). The neurobiology of slow synaptic transmission. *Science*, **294**, 1024–1030.
- Angers-Loustau, A., Cote, J. F. & Tremblay, M. L. (1999). Roles of protein tyrosine phosphatases in cell migration and adhesion. *Biochem. Cell Biol.* **77**, 493–505.
- Benkovic, S. J. & Schray, K. J. (1978). The mechanism of phosphoryltransfer. In *Transition States of Biochemical Processes* (Gandour, E. D., ed.), pp. 492–572, Plenum Press, New York.
- Admiraal, S. J. & Herschlag, D. (1995). Mapping the transition state for ATP hydrolysis: implications for enzymatic catalysis. *Chem. Biol.* **2**, 729–739.
- Aqvist, J., Kolmodin, K., Florian, J. & Warshel, A. (1999). Mechanistic alternatives in phosphate monoester hydrolysis: what conclusions can be drawn from available experimental data? *Chem. Biol.* **6**, R71–R80.
- Mildvan, A. S. (1997). Mechanisms of signaling and related enzymes. *Proteins: Struct. Funct. Genet.* **29**, 401–416.
- Warshel, A. & Florian, J. (1998). Computer simulations of enzyme catalysis: finding out what has been optimized by evolution. *Proc. Natl Acad. Sci. USA*, **95**, 5950–5955.
- Zhang, Z. Y. (1998). Protein-tyrosine phosphatases: biological function, structural characteristics, and mechanism of catalysis. *Crit. Rev. Biochem. Mol. Biol.* **33**, 1–52.
- Collet, J. F., Stroobant, V., Pirard, M., Delpierre, G. & Van Schaftingen, E. (1998). A new class of phosphotransferases phosphorylated on an aspartate residue in an amino-terminal DXDX(T/V) motif. *J. Biol. Chem.* **273**, 14107–14112.
- Ridder, I. S. & Dijkstra, B. W. (1999). Identification of the  $\text{Mg}^{2+}$ -binding site in the P-type ATPase and phosphatase members of the HAD (haloacid dehalogenase) superfamily by structural similarity to the response regulator protein CheY. *Biochem. J.* **339**, 223–226.
- Matsui, T., Sekiguchi, M., Hashimoto, A., Tomita, U., Nishikawa, T. & Wada, K. (1995). Functional comparison of D-serine and glycine in rodents: the effect on cloned NMDA receptors and the extracellular concentration. *J. Neurochem.* **65**, 454–458.
- Berger, A. J., Dieudonne, S. & Ascher, P. (1998). Glycine uptake governs glycine site occupancy at NMDA receptors of excitatory synapses. *J. Neurophysiol.* **80**, 3336–3340.
- Sugiura, N., Patel, R. G. & Corriveau, R. A. (2001). N-Methyl-D-aspartate receptors regulate a group of transiently expressed genes in the developing brain. *J. Biol. Chem.* **276**, 14257–14263.
- Cho, H. S., Wang, W., Kim, R., Yokota, H., Damo, S., Kim, S.-H. *et al.* (2001).  $\text{BeF}_3^-$  acts as a phosphate analog in proteins phosphorylated on aspartate: structure of a  $\text{BeF}_3^-$  complex with phosphoserine phosphatase. *Proc. Natl Acad. Sci. USA*, **98**, 8525–8530.
- Wang, W., Kim, R., Jancarik, J., Yokota, H. & Kim, S.-H. (2001). Crystal structure of phosphoserine phosphatase from *Methanococcus jannaschii*, a hyperthermophile, at 1.8 Å resolution. *Struct. Fold. Des.* **9**, 65–71.
- Pannifer, A. D., Flint, A. J., Tonks, N. K. & Barford, D. (1998). Visualization of the cysteinyl-phosphate

- intermediate of a protein-tyrosine phosphatase by X-ray crystallography. *J. Biol. Chem.* **273**, 10454–10462.
23. Scheffzek, K., Ahmadian, M. R., Kabsch, W., Wiesmuller, L., Lautwein, A., Schmitz, F. & Wittinghofer, A. (1997). The Ras–RasGAP complex: structural basis for GTPase activation and its loss in oncogenic Ras mutants. *Science*, **277**, 333–338.
24. Richards, F. M. & Kundrot, C. E. (1988). Identification of structural motifs from protein coordinate data: secondary structure and first-level supersecondary structure. *Proteins: Struct. Funct. Genet.* **3**, 71–84.
25. Collet, J. F., Stroobant, V. & Van Schaftingen, E. (1999). Mechanistic studies of phosphoserine phosphatase, an enzyme related to P-type ATPases. *J. Biol. Chem.* **274**, 33985–33990.
26. Lowry, T. H. & Richardson, K. S. (1987). *Mechanism and Theory in Organic Chemistry*, 3rd edit., Harper and Row, New York.
27. Jencks, W. P. (1987). *Catalysis in Chemistry and Enzymology*, Dover, New York.
28. Williams, A. (1992). Effective charge and transition-state structure in solution. *Advan. Phys. Org. Chem.* **27**, 1–55.
29. Toyoshima, C., Nakasako, M., Nomura, H. & Ogawa, H. (2000). Crystal structure of the calcium pump of sarcoplasmic reticulum at 2.6 Å resolution. *Nature*, **405**, 647–655.
30. Stock, A. M., Mottonen, J. M., Stock, J. B. & Schutt, C. E. (1989). Three-dimensional structure of CheY, the response regulator of bacterial chemotaxis. *Nature*, **337**, 745–749.
31. Djordjevic, S., Goudreau, P. N., Xu, Q., Stock, A. M. & West, A. H. (1998). Structural basis for methyl-esterase CheB regulation by a phosphorylation-activated domain. *Proc. Natl Acad. Sci. USA*, **95**, 1381–1386.
32. Volkman, B. F., Nohaile, M. J., Amy, N. K., Kustu, S. & Wemmer, D. E. (1995). Three-dimensional solution structure of the N-terminal receiver domain of NTRC. *Biochemistry*, **34**, 1413–1424.
33. Baikalov, I., Schroder, I., Kaczor-Grzeskowiak, M., Grzeskowiak, K., Gunsalus, R. P. & Dickerson, R. E. (1996). Structure of the *Escherichia coli* response regulator NarL. *Biochemistry*, **35**, 11053–11061.
34. Gouet, P., Fabry, B., Guillet, V., Birck, C., Mourey, L., Kahn, D. & Samama, J. P. (1999). Structural transitions in the FixJ receiver domain. *Struct. Fold. Des.* **7**, 1517–1526.
35. Muller-Dieckmann, H. J., Grantz, A. A. & Kim, S. H. (1999). The structure of the signal receiver domain of the *Arabidopsis thaliana* ethylene receptor ETR1. *Struct. Fold. Des.* **7**, 1547–1556.
36. Lewis, R. J., Brannigan, J. A., Muchova, K., Barak, I. & Wilkinson, A. J. (1999). Phosphorylated aspartate in the structure of a response regulator protein. *J. Mol. Biol.* **294**, 9–15.
37. Sola, M., Gomis-Ruth, F. X., Serrano, L., Gonzalez, A. & Coll, M. (1999). Three-dimensional crystal structure of the transcription factor PhoB receiver domain. *J. Mol. Biol.* **285**, 675–687.
38. Andersen, J. P. (1995). Dissection of the functional domains of the sarcoplasmic reticulum  $\text{Ca}^{2+}$ -ATPase by site-directed mutagenesis. *Biosci. Rep.* **15**, 243–261.
39. Tanford, C., Reynolds, J. A. & Johnson, E. A. (1987). Sarcoplasmic reticulum calcium pump: a model for  $\text{Ca}^{2+}$  binding and  $\text{Ca}^{2+}$ -coupled phosphorylation. *Proc. Natl Acad. Sci. USA*, **84**, 7094–7098.
40. Kobor, M. S., Archambault, J., Lester, W., Holstege, F. C., Gileadi, O., Jansma, D. B. *et al.* (1999). An unusual eukaryotic protein phosphatase required for transcription by RNA polymerase II and CTD dephosphorylation in *S. cerevisiae*. *Mol. Cell*, **4**, 55–62.
41. Siniosoglou, S., Hurt, E. C. & Pelham, H. R. (2000). Psr1p/Psr2p, two plasma membrane phosphatases with an essential DXDX(T/V) motif required for sodium stress response in yeast. *J. Biol. Chem.* **275**, 19352–19360.
42. Fuchs, T., Wiget, P., Osteras, M. & Jenal, U. (2001). Precise amounts of a novel member of a phosphotransferase superfamily are essential for growth and normal morphology in *Caulobacter crescentus*. *Mol. Microbiol.* **39**, 679–692.
43. Fallon, H. J., Hackney, E. J. & Byrne, W. L. (1966). Serine biosynthesis in rat liver. Regulation of enzyme concentration by dietary factors. *J. Biol. Chem.* **241**, 4157–4167.
44. Chen, P. S., Toribara, T. Y. & Warner, H. (1956). Microdetermination of phosphorus. *Anal. Chem.* **28**, 1756–1758.
45. Otwinowski, Z. & Minor, W. (1996). Processing of X-ray diffraction data collected in oscillation mode. *Methods Enzymol.* **276**, 307–326.
46. Navaza, J. (1994). AMoRe: an automated package for molecular replacement. *Acta Crystallog. sect. A*, **50**, 157–163.
47. Brünger, A. T., Adams, P. D., Clore, G. M., DeLano, W. L., Gros, P., Grosse-Kunstleve, R. W. *et al.* (1998). Crystallography and NMR system: a new software suite for macromolecular structure determination. *Acta Crystallog. sect. D*, **54**, 905–921.
48. Jones, T. A., Zou, J.-Y., Cowan, S. W. & Kjeldgaard, M. (1991). Improved methods for building protein models in electron density maps and the location of errors in these models. *Acta Crystallog. sect. A*, **47**, 110–119.

Edited by D. Rees

(Received 6 December 2001; received in revised form 20 March 2002; accepted 5 April 2002)